Adiabatic hyperspherical study of the helium trimer

B. D. Esry, C. D. Lin,* and Chris H. Greene
Department of Physics and JILA,University of Colorado, Boulder, Colorado 80309-0440
(Received 19 March 1996)

The adiabatic hyperspherical method is used to investigate the spectrum of the helium trimer and to explore effects on the spectrum of varying the helium masses as well as the interaction strength. When a realistic helium dimer potential is adopted, only two isotopic combinations are observed to have three-body bound states: $^4He_3$ and $^4He_2\,^3He$. By artificially adjusting the dimer potential, we also determine the range of interaction strengths for which halo states can result. The existence of Efimov states for both physical and unphysical systems is also examined.

PACS number(s): 31.15.Ja, 36.90.+f

I. INTRODUCTION

A curious property of three-body systems is that they can form bound states even when none exist for the separate two-body subsystems. This situation occurs for the striking cases of Efimov [1–3] and halo (or Borromean) [4–8] states. Both types of states can exist in systems of identical particles (symmetric systems) and can, in principle, exist in systems of different particles (asymmetric systems) [2,5]. In this paper we focus on the simpler case of identical particles, however, except when we explicitly state otherwise. (The reader is encouraged to keep in mind that all of the statements have generalizations that apply to asymmetric systems.)

Both Efimov and halo states occur only in systems which interact *via* potentials which fall off faster than r^{-2}. The distinction between the two lies in the two-body spectrum: Efimov states result when there is a zero (or near zero) energy two-body bound state whereas halo states result when there are *no* two-body bound states. While examples of halo states have been studied in models of nuclei [6–9], they have not been carefully studied in either atomic or molecular systems. Further, no clear example of Efimov states exist in any field. These exotic states will not exist in any atom because of the presence of long range Coulomb interactions, but might exist in systems of neutral atoms due to the rapid decrease of the neutral diatom interaction potential with internuclear distance.

As noted by several authors [3,10–16], one excellent candidate in this category is ^{4}He since the dimer, $^4He_2$, is predicted to have only one weakly bound state [12,13,17–20] ($E_0 \approx 1$ mK).[1] Because the dimer is so weakly bound, it is difficult to detect and has, in fact, only recently been observed experimentally by Luo *et al.* [21,22]. In a subsequent and independent experiment, Schöllkopf and Toennies [23,24] were able to see not only the helium dimer, but also the trimer and tetramer. Unfortunately, no experiment has been able to verify the existence of an Efimov state in the helium trimer even though an Efimov state was predicted for this system by Lim *et al.* [14]. Lim *et al.* found two bound states for the trimer, of which the first excited state was claimed to be an Efimov state. Subsequent calculations [12,13,15,16] gave a ground state plus zero, one, or two Efimov states. Much of the controversy was due to uncertainties in the helium dimer potential since the number of Efimov states is very sensitive to the binding energy of the dimer. For instance, a decrease of between 1% and 2% in the dimer interaction strength for a typical potential available at the time of the calculations [25] results in a second Efimov state [12], and a decrease of 2.08% results in an infinite number of Efimov states.

In recent years, more accurate helium dimer potentials [18,20,26] have become available which are consistent with each other as well as with experimental measurements of virial coefficients and viscosities over a wide range of temperatures. Using one of these potentials [26], we find a single Efimov state. Decreasing the interaction strength still further places the system in the domain of halo states since there are no longer any two-body bound states. We find that halo states persist until the depth of the dimer interaction potential has been decreased by between 10% and 14%.

We begin by examining the bound states of the trimer of ^{4}He. This system has been studied theoretically with the hope of finding a physical example of an Efimov state [14–16]. In our study, we also examine the systems $^4He_2\,^3He$, $^4He\,^3He_2$, and $^3He_3$ to provide contrast for $^4He_3$ and to show the effects on the three-body spectrum of varying the masses in the system. In addition, we artificially vary the interaction strength for $^4He_3$ in order to show that Efimov's result [1–3,7,10,11] holds for a realistic neutral atom interaction potential. We further determine the range of interaction strengths which result in halo states.

II. METHOD

We solve the Schrödinger equation for three interacting helium atoms using the adiabatic hyperspherical method [27,28]. We consider only the most favorable conditions for Efimov states, namely $L=0$ and a spatial wave function symmetric under interchange of identical particles [2]. The condition of zero total angular momentum insures that for the lowest states the long-range centrifugal potentials do not

*Present address: Institute of Physics, National Chiao-Tung University, Hsinchu, Taiwan.

[1]In references on this topic, the binding energy is often reported in terms of degrees Kelvin. The conversion is 1 K = $3.166\,829\times10^{-6}$ a.u.

dominate the short-range interparticle interactions; the symmetry condition is merely a reflection of the fact that we seek loosely bound states which might not be bound for antisymmetric states due to the higher kinetic energy associated with the extra node.

We proceed by first writing the Schrödinger equation in terms of Jacobi coordinates to eliminate the trivial center of mass motion (see Refs. [27,28]). The Jacobi coordinates we use are $\boldsymbol{\rho}_1$, the vector from particle 1 to particle 2, and $\boldsymbol{\rho}_2$, the vector from the center of mass of the first pair to particle 3. We then transform to mass-weighted hyperspherical coordinates [27]. In this coordinate system, all coordinates save one (the hyperradius R) are ''angular,'' i.e., limited to a finite range. The transformation to mass-weighted hyperspherical coordinates is given by

$$\mu R^2=\mu_1\rho_1^2+\mu_2\rho_2^2,$$

$$\tan\phi=\sqrt{\frac{\mu_2}{\mu_1}}\frac{\rho_2}{\rho_1},$$

and

$$\cos\theta=\frac{\boldsymbol{\rho}_1\cdot\boldsymbol{\rho}_2}{\rho_1\rho_2}.$$

In these expressions, μ is an arbitrary scaling factor which we choose to be the reduced mass of the identical pair of particles. For example, for $^4He_3$ we use the reduced mass of $^4He_2$; and for $^4He\,^3He_2$, the reduced mass of $^3He_2$. The reduced masses associated with the Jacobi coordinates $\boldsymbol{\rho}_1$ and $\boldsymbol{\rho}_2$ are

$$\frac{1}{\mu_1}=\frac{1}{m_1}+\frac{1}{m_2}$$

and

$$\frac{1}{\mu_2}=\frac{1}{m_1+m_2}+\frac{1}{m_3}.$$

In general, three Euler angles are also needed to describe the orientation of the plane of the particles. However, since we only consider zero total orbital angular momentum, the Euler angle dependence drops out. The Schrödinger equation then involves only the three internal coordinates R, ϕ, and θ (in atomic units) [27–29],

$$\left(-\frac{1}{2\mu}\frac{\partial^2}{\partial R^2}+\frac{\Lambda^2-\frac{1}{4}}{2\mu R^2}+V(R,\phi,\theta)\right)\psi=E\psi. \qquad (1)$$

Here, Λ^2 is the ''grand angular momentum'' operator [27,29]

$$\Lambda^2=-\frac{\partial^2}{\partial\phi^2}-\frac{1}{\sin\phi\cos\phi\sin\theta}\frac{\partial}{\partial\theta}\left(\sin\theta\frac{\partial}{\partial\theta}\right).$$

Note also that the wave function $\psi(R,\phi,\theta)$ is rescaled from the ''true wave function'' by a factor $R^{5/2}\sin\phi\cos\phi$ in order to eliminate first derivatives from the kinetic energy operator. The rescaled wave function must be square integrable for a bound state, and it must obey the boundary conditions

$$\psi(0,\phi,\theta)=0,$$

$$\psi(R,0,\theta)=\psi\left(R,\frac{\pi}{2},\theta\right)=0,$$

and

$$\left.\frac{\partial\psi}{\partial\theta}\right|_{\theta=0}=\left.\frac{\partial\psi}{\partial\theta}\right|_{\theta=\pi}=0.$$

In the adiabatic approach, we treat R initially as a fixed parameter and solve the remaining eigenvalue equation as

$$\left(\frac{\Lambda^2-\frac{1}{4}}{2\mu R^2}+V\right)\Phi_\nu(R;\phi,\theta)=U_\nu(R)\Phi_\nu(R;\phi,\theta). \qquad (2)$$

From the definitions of the coordinates, we see that R gives the overall scale of the three-body system; ϕ, the radial correlation; and θ, the angular correlation. Further, R is completely symmetric under particle permutations. It follows that the solutions $\Phi_\nu(R;\phi,\theta)$ — the channel functions — contain all of the identical particle symmetries as well as all of the correlations in the system. Because of this, the channel functions display much of the physical content of the total wave function, and we will often use them to obtain a qualitative understanding of the dynamics.

We solve Eq. (2) using the finite element method [28], thus determining adiabatic potential curves $U_\nu(R)$ and a set of orthonormal channel functions $\Phi_\nu(R;\phi,\theta)$ that depend parametrically on R. As in Ref. [28], we expand the channel functions in each element on a product basis of fifth order Hermite interpolating polynomials in ϕ and θ [30]. We choose the elements to be rectangular with a nonuniform distribution in the (ϕ,θ) plane. In the calculation, we use from 560 elements for small R to 1320 elements for large R. This leads to matrices of order 8960 and 21120, respectively, of which less than about 2% of the entries are nonzero. We are able to diagonalize these large sparse matrices on workstations by using the LANZ package [31,32] which is based upon the Lanczos algorithm [33]. This provides an efficient means of obtaining the lowest eigenvalues and eigenvectors (potential curves and channel functions) of the adiabatic equation, Eq. (2).

The full solution to the Schrödinger equation is found in the adiabatic approximation by writing

$$\psi(R,\phi,\theta)=\sum_\nu F_\nu(R)\Phi_\nu(R;\phi,\theta),$$

substituting in Eq. (1), and neglecting coupling between different channels arising from the nonvanishing derivatives of the channel functions with respect to R. The Schrödinger equation reduces to

$$\left(-\frac{1}{2\mu}\frac{d^2}{dR^2}+U_\nu(R)+W_{\nu\nu}(R)\right)F_{\nu n}(R)=E_{\nu n}F_{\nu n}(R) \qquad (3)$$

where

$$W_{\nu\nu}(R) = -\frac{1}{2\mu}\left\langle \Phi_\nu(R)\left|\frac{d^2}{dR^2}\right|\Phi_\nu(R)\right\rangle .$$

This is a one-dimensional radial Schrödinger equation with an effective hyperradial potential $U_\nu(R)+W_{\nu\nu}(R)$ that determines the three-body spectrum in the adiabatic approximation. It can be shown [34] that the ground-state energy obtained by solving Eq. (3) is an upper bound to the true ground-state energy. This can be simply understood from the fact this approach is equivalent to assuming a variational trial wave function of the form

$$\psi^t_{\nu n}(R,\phi,\theta) = F_{\nu n}(R)\Phi_\nu(R;\phi,\theta).$$

The variational principle then guarantees that the energy thus obtained is an upper bound to the true ground-state energy. A further approximation may be made in Eq. (3) by which we can also determine a lower bound to the ground-state energy [34]. We only need to neglect $W_{\nu\nu}(R)$. This corresponds to the familiar Born-Oppenheimer approximation. However, the energy calculated variationally is often much closer to the actual energy than is the lower bound. So, while we quote both the upper and lower bounds, we base our conclusions upon the upper bounds.

A principal advantage of the adiabatic hyperspherical method is the reduction of a multidimensional problem to a one-dimensional problem with a set of effective potentials [27]. These potential curves provide a great deal of qualitative as well as quantitative information about the dynamics of the system and often give a convenient and useful classification scheme [27]. The utility and importance of a qualitative approach to three-body dynamics is clear and has been emphasized by Efimov [3]. His analysis was limited to sketching potential curves for resonant cases only. That is, three-body systems for which one or more of the two-body subsystems has a zero or near zero energy bound state. In contrast, the adiabatic hyperspherical method provides a framework within which one can usually sketch semiquantitative potential curves for more general cases without resorting to complicated numerical calculations. Momentum space Fadeev approaches [12], on the other hand, do not provide for the calculation of potential curves. One can, however, adopt an adiabatic approximation (as we do) and calculate potential curves in the coordinate space Fadeev approach [9].

To construct $V(R;\phi,\theta)$ in Eq. (2), we assume that the three helium atoms interact solely through the pairwise sum of the helium dimer potential. That is, we neglect any inherently three-body terms in the potential such as the Axilrod-Teller dipole-dipole-dipole dispersion term [35]. It is a short range correction (proportional to R^{-9}) and does not effect the long range behavior of the effective hyperradial potential that is important for the loosely bound states we study. In fact, such corrections to pairwise additivity have been studied for the helium trimer and have been shown to contribute less than 1% to the ground-state energy [36,37]. For the dimer potential we use the convenient and accurate representation of Aziz *et al.* [26] (in their paper, this is the potential designated LM2M2 with add-on),

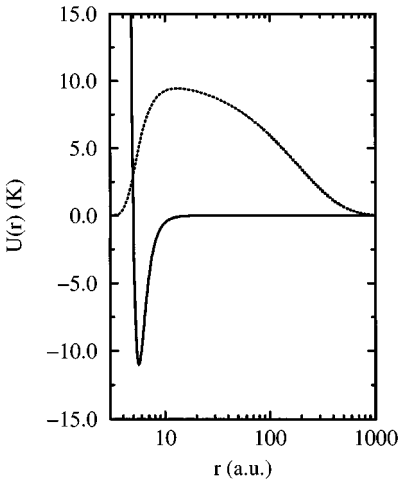

FIG. 1. The helium dimer interaction potential (solid line) and ground-state wave function (dotted line).

$$U(r) = \epsilon\left[A\exp(-\alpha x-\beta x^2) - \left(\frac{c_6}{x^6}+\frac{c_8}{x^8}+\frac{c_{10}}{x^{10}}\right)F(x)+BU_{ao}(x)\right]$$

where r is the interatomic distance,

$$x = \frac{r}{r_{min}},$$

$F(x)$ is a cutoff function given by

$$F(x) = \begin{cases} e^{-(D/x-1)^2}, & x<D \\ 1, & x\geq D \end{cases}$$

and $U_{ao}(x)$ is an add-on term given by

$$U_{ao}(x) = \sin\left[\frac{2\pi(x-x_0)}{x_1-x_0}-\frac{\pi}{2}\right]+1.$$

With this potential they were able to reproduce a variety of experimental data within the experimental error bars while maintaining consistency with *ab initio* potential curves [16,18,20]. The parameters in $U(r)$ are as follows [26]:

$\epsilon = 10.97$ K, $A = 1.896\,353\,53\times10^5$, $\alpha = 10.702\,035\,39$,

$\beta = 1.907\,406\,49$, $c_6 = 1.346\,870\,65$, $c_8 = 0.413\,083\,98$,

$c_{10} = 0.170\,601\,59$, $D = 1.4088$, $r_{min} = 5.6115$ a.u.,

$B = 0.0026$, $x_0 = 1.003\,535\,949$, $x_1 = 1.454\,790\,369$.

The ground state of the helium dimer calculated using this potential is indeed loosely bound as evidenced by a binding energy of 1.310 mK and by the large spatial extent of the wave function (see Fig. 1). The mean value of r is approximately 100 a.u. prompting the claim that the helium dimer is the largest diatomic molecule [23]. Given the size of the molecule, retardation effects might be expected to have a noticeable effect. One calculation has, in fact, indicated as

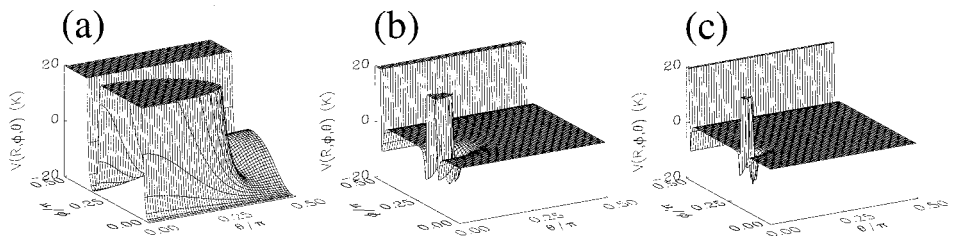

FIG. 2. Three-body potential surfaces for R values of (a) 12 a.u., (b) 50 a.u., and (c) 100 a.u.

much as a 12% decrease in the binding energy of the dimer [38]. Nevertheless, we neglect retardation corrections in our calculation and delay speculation on their possible effects on the three-body spectrum to Sec. III.

III. RESULTS AND DISCUSSION

A. Bound states versus interaction strength

It is useful at this point to describe qualitatively the three-body spectrum in relation to the two-body spectrum as a function of the two-body interaction strength. This will make clear the relation between Efimov states, halo states, and ''normal'' states as well as the progression from one type to the next as the interaction strength changes. So, let us consider a system which interacts through the attractive, short range, two-body potential $\lambda U(r)$ with λ a constant which fixes the interaction strength. We will take $\lambda=1$ to be the physical value. The three-body interaction in our approximation is then

$$V(R,\phi,\theta)=\lambda[U(r_{12})+U(r_{23})+U(r_{31})]$$

and is plotted for $\lambda=1$ for various values of R in Fig. 2. In this and all subsequent surface plots, we show half of the (ϕ,θ) plane as all of the systems we consider are symmetric about $\theta=\pi/2$. From the definition of the coordinates, for a given hyperradius the interparticle coordinates r_{ij} cover the range 0 to R. Also, $r_{12}=0$ along the line $\phi=\pi/2$, $r_{23}=0$ at the point $(\phi=\pi/6,\theta=0)$, and $r_{31}=0$ at the point $(\phi=\pi/6,\theta=\pi)$ from symmetry. So, in Fig. 2(a), we see that the large repulsive part of the dimer potential dominates in a large fraction of the (ϕ,θ) plane around $r_{ij}=0$, but as R increases [Figs. 2(a) and 2(b)] this region shrinks around $r_{ij}=0$ since the interparticle distances cover larger ranges.

We show in Fig. 3 the binding energies for $^4He_3$ as a function of λ. For $\lambda<\lambda_{\rm Efimov}$, $E=0$ corresponds to three free atoms while for $\lambda>\lambda_{\rm Efimov}$, $E=0$ corresponds to one atom free relative to two bound atoms. This figure illustrates the following discussion.

Starting at the free particle limit, $\lambda=0$, there are neither two-body nor three-body bound states. Increasing λ, we find that three-body bound states begin appearing at some value of λ, $\lambda_{\rm halo}$ (the dotted line in Fig. 3). It is because these three-body bound states exist when there are no two-body bound states that they are called halo states. They remain and their number increases until λ reaches a value $\lambda_{\rm Efimov}$ (the dashed line in Fig. 3) for which there is a zero energy two-body s-wave bound state. As λ increases toward $\lambda_{\rm Efimov}$, the number of three-body bound states increases rapidly becoming infinite at $\lambda=\lambda_{\rm Efimov}$ and then decreases rapidly as λ increases beyond $\lambda_{\rm Efimov}$. In the region $\lambda\approx\lambda_{\rm Efimov}$, the three-body states typically have very large spatial extent.

The ground-state energy for the three-body system decreases as λ increases through the halo region to the Efimov limit regardless of the number of bound states. As λ increases beyond $\lambda_{\rm Efimov}$, the three-body ground-state energy continues to decrease even as the number of three-body bound states diminishes. This is a somewhat remarkable property of Efimov states and is worth repeating: starting from $\lambda_{\rm Efimov}$, the number of three-body bound states decreases as the interaction strength, λ, increases. This is, in fact, the defining quality of Efimov states. The states which disappear are Efimov states while any states which remain are normal states. This is shown clearly in Fig. 3. The first excited state passes into the continuum at $\lambda\approx1.2$ while the ground state remains bound. The explanation for the reduction in the number of bound states is that for $\lambda>\lambda_{\rm Efimov}$ there is one two-body bound state whose energy decreases faster than the energy of the excited three-body states as a function of λ. In the language of potential curves, this process can be understood as the two-body threshold (the asymptotic value of the three-body potential) moving down in energy faster than the three-body energy levels in the potential as a function of λ. Thus, any high lying Efimov states pass sequentially into the three-body continuum as λ gets larger.

If we continue to increase λ until the energy of the first excited state of the dimer is zero, we will again find an infinite number of Efimov states lying below this threshold. However, they will no longer be true three-body bound

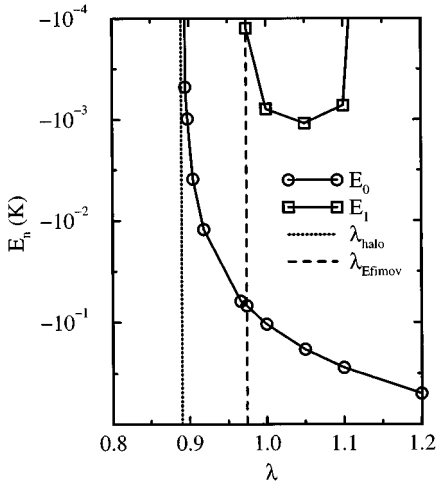

FIG. 3. The trimer binding energies as a function of the interaction strength, λ, for the physical value $\lambda=1$. Shown are $\lambda=\lambda_{\rm halo}=0.89$ (dotted line), $\lambda=\lambda_{\rm Efimov}=0.9741$ (dashed line), the ground state (circles), and the first excited state (squares).

states, but rather three-body resonances. In addition, there will be some finite number of normal three-body bound states lying at lower energies. For example, we found that for $\lambda = 6.823$ the ground state of the dimer is relatively securely bound ($E_0 = -26$ K) and the first excited state has zero energy. For this value of λ, the trimer has five normal bound states which asymptotically go to the dimer in the ground state plus a free helium atom. The next group of states is an infinite number of Efimov resonances which asymptotically go to three free atoms. They are resonances rather than true bound states since they belong to a potential curve from which they can decay into the continuum of a lower curve *via* nonadiabatic coupling. A further increase in λ causes the binding energy of the first excited two-body state to increase and eventually brings the energy of the second excited state to zero which again results in an infinite set of Efimov resonances. The process continues and repeats itself each time there is a zero energy bound state.

B. Efimov states in the helium trimer

As mentioned above, Efimov states are characterized by the peculiar fact that their number increases as the two-body potential strength approaches the value which gives a zero energy two-body bound state. In this limit, they become dipole states and thus very diffuse — the expectation value of r increases exponentially with vibrational quantum number [39–41]. In the adiabatic hyperspherical approach, the Efimov case manifests itself in the channel functions Φ_ν as an almost equal probability for being in the region between nuclei and the region near nuclei (see Sec. B 3 and Fig. 10 below) for all R. By contrast, the channel functions for normal states show a collapse of the probability density into the two-body potential wells as R increases. From the three-body potential surfaces in Fig. 2, we see that the two-body potential well becomes increasingly localized in ϕ and θ as R increases which forces any bound diatomic molecular state to do the same. Physically, this corresponds to one atom being far from the remaining two which are bound in a diatomic molecular state.

1. The ^{4}He trimer

For $^4\mathrm{He}_3$ we first performed the calculation with the helium dimer potential [25] available to Cornelius and Glöckle [12] in order to compare with their results. They also solved the three-body Schrödinger equation, but from the very different approach of using a Fadeev decomposition of the wave function in momentum space. They further expanded the Fadeev components written in Jacobi coordinates in partial waves including s and d waves. Using a mass of 7296.3 a.u. for ^{4}He, we calculate a dimer binding energy of 0.8352 mK which is in agreement with their result (see also [19]). For the trimer, we find (lower bounds in parentheses) $E_0 = -0.09811$ K (-0.2770 K) and $E_1 = -1.517$ mK (-2.693 mK) where they obtained $E_0 = -0.11$ K and $E_1 = -1.6$ mK. Thus, our results for the three-body system are also in good agreement. By noting the disappearance of the three-body excited state as the interaction strength was increased, they were able to identify the first excited state as being an Efimov state. However, by simultaneously adjusting the potential depth and equilibrium distance within the quoted error bars of the potential, they found that it was possible to bind an additional Efimov state.

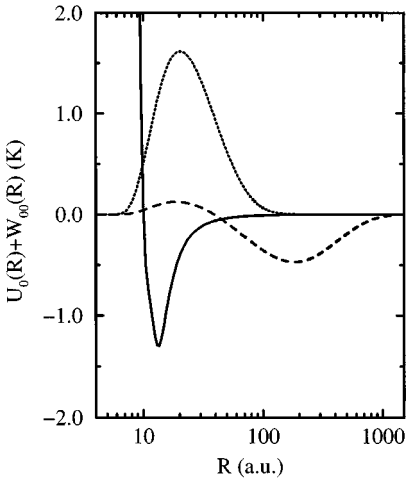

FIG. 4. The $^4\mathrm{He}_3$ effective hyperradial potential curve (solid line), ground-state wave function (dotted line), and first excited state wave function (dashed line). Notice that the hyperradius has a logarithmic scale.

We repeated the calculations using an improved dimer potential [26] which gives a binding energy for $^4\mathrm{He}_2$ of 1.310 mK — a 57% increase. Though deeper, the improved interaction potential does not yield any more three-body bound states, but the energies of the trimer are shifted to $E_0 = -0.1061$ K (-0.2937 K) and $E_1 = -2.118$ mK (-3.518 mK) which translates into a 6% to 8% change for the ground state and a 30% to 40% change for the first excited state. The greater sensitivity of the first excited state to the change in the potential might be interpreted as evidence for its being an Efimov state. This is somewhat misleading, though, since the two potentials differ by more than a simple factor. Thus, the results from the two potentials cannot be directly compared to determine the existence of an Efimov state. We do find, however, that increasing the interaction strength of the improved potential by a factor of about 1.2 (see Fig. 3) causes the first excited state to become unbound, and thus it is a genuine Efimov state within the adiabatic approximation. We show the results for the physical interaction strength, $\lambda = 1$, in Fig. 4. We plot the effective hyperradial potential curve as well as the wavefunctions for the

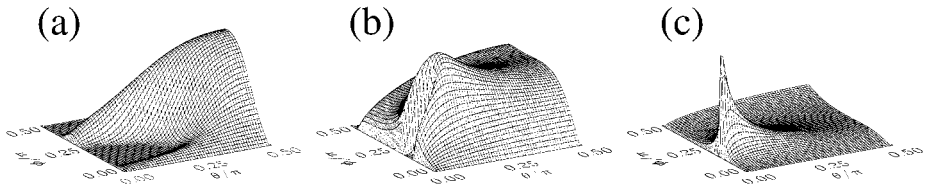

FIG. 5. The channel functions for $^4\mathrm{He}_3$ plotted as $\sin\theta|\Phi_\nu(R;\phi,\theta)|^2$ for (a) $R = 12$ a.u., (b) $R = 50$ a.u., and (c) $R = 500$ a.u. The vertical axis is a square-root scale.

ground and first excited states. Notice that the hyperradial axis has a logarithmic scale showing the extremely large spatial extent of the first excited state, an Efimov state.

We plot the channel functions for various values of R in Fig. 5. The surfaces in this and subsequent figures are the absolute square of the channel functions including the volume element. Notice that the probability distribution for Figs. 5(a) ($R=12$ a.u.) and 5(b) ($R=50$ a.u.) is quite similar to that expected for Efimov states in that the channel function has large probability for being in the region between the nuclei as well in the region near the nuclei. At larger hyperradii, as seen in Fig. 5(c) at $R=500$ a.u., the channel function is concentrated near the two-body potential wells and is essentially the dimer ground state wave function. As we will see in Fig. 10, for the true Efimov state, the channel function at large R is not localized in the two-body potential wells even asymptotically.

We have seen that the trimer binding energies are quite sensitive to the binding energy of the dimer. For this reason, the 12% decrease in the dimer binding energy calculated by Luo *et al.* [38] due to retardation effects would probably have a 10% effect on the energy of the first excited state of the trimer. It is doubtful, however, that this is sufficient to change the number of bound states of the trimer or the character of the first excited state. Roughly speaking, a decrease of nearly 60% (from the new dimer potential to the old) was not enough to add another Efimov state. So, while the effects of retardation move the dimer binding energy in the right direction for adding Efimov states, we expect that it is insufficient to change our conclusions for $^4He_3$.

2. Other helium isotope trimers

To study the variation of the three-body spectrum with the masses of the particles, we performed the calculations for the $^4He_2{}^3He$, $^4He\,^3He_2$, and $^3He_3$ systems. We considered only the nodeless solutions of Eq. (2). For the asymmetric systems, this is consistent with symmetrization requirements. However, for the trimer of ^3He, a fermion, this is an unphysical state since it is not possible to form the totally antisymmetric spin state for three spin-1/2 particles that would be required to satisfy the Pauli principle with a totally symmetric spatial wave function. We ignore this problem and include $^3He_3$ for completeness realizing that this case is purely of theoretical interest. Using a mass of 5497.9 a.u. for ^3He, we find that there are no bound states for either of the dimers $^4He^3He$ or $^3He_2$.

The effective hyperradial potentials $U_0(R)+W_{00}(R)$ for all three-body systems considered are shown in Fig. 6. We see that the two systems with lighter particles exhibit a barrier while the other two do not. This is consistent with previous calculations [42] which examined the dependence of three-body potentials on the strength of the two-body interactions for short range model potentials. Given that the three-body potentials for $^4He\,^3He_2$ and $^3He_3$ have only a shallow and narrow attractive well compared to $^4He_3$ and that the heavier $^4He_3$ has only two bound states, it is not surprising that only $^4He_2{}^3He$ has three-body bound states. Its single bound state has an energy of $E_0=-0.01022$ K (-0.08652 K).

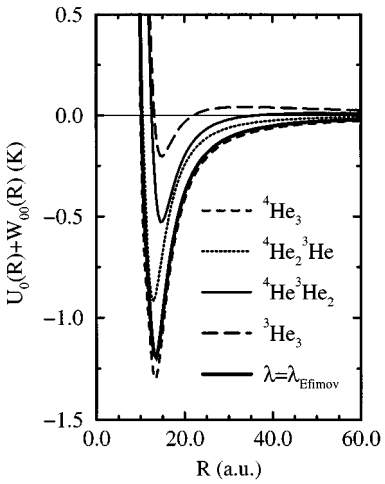

FIG. 6. The adiabatic hyperspherical potential curves for the physical systems $^4He_3$ (solid line), $^4He_2\,^3He$ (dotted line), and $^4He\,^3He_2$ (dashed line) as well as the nonphysical systems $^3He_3$ (long dashed line) and $\lambda=\lambda_{\rm Efimov}$ (thick solid line).

We show in Fig. 7 the $^3He_3$ channel functions for various R values. These should be compared to the lowest hyperspherical harmonic in Fig. 8 which is the solution to Eq. (1) in the absence of interactions (see Ref. [27]). For R values beyond the barrier maximum, the similarity of the channel functions for $^3He_3$ and the lowest hyperspherical harmonic suggests that the three helium atoms behave largely as free particles. The channel functions for $^4He\,^3He_2$ are very similar to those for $^3He_3$ just as those for $^4He_2\,^3He$ are similar to $^4He_3$.

3. The $\lambda=\lambda_{\rm Efimov}$ case

To complete our study of Efimov states for the helium trimer, we reduced the interaction strength from its physical value until the dimer bound-state energy was zero. As explained above, this should lead to an infinite number of states, and indeed it does because for this specific case, the effective potential is proportional to R^{-2} and attractive. The interaction strength needs only to be reduced by 2.59% to reach this case. The calculated effective potential agrees well with the anticipated result and is also shown in Fig. 9. We plot $R^2U_0(R)$ versus R^{-1} in Fig. 9 to more clearly show the asymptotic behavior. A potential with leading terms propor-

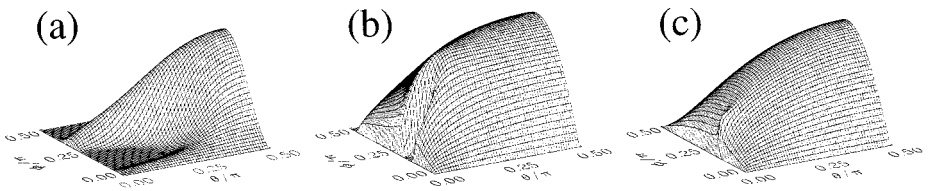

FIG. 7. The channel functions for $^3He_3$ plotted as $\sin\theta|\Phi_\nu(R;\phi,\theta)|^2$ for (a) $R=12$ a.u., (b) $R=50$ a.u., and (c) $R=500$ a.u. The vertical axis is a square-root scale.

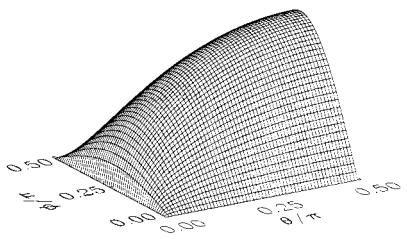

FIG. 8. The lowest hyperspherical harmonic plotted as $\sin\theta|u_{[0]}(\phi,\theta)|^2$. The vertical axis is a square-root scale.

tional to R^{-2} and R^{-3} asymptotically will appear as straight lines with this rescaling and change of variable. By fitting a line to the calculated points, we can extract the coefficient of the R^{-2} term to compare with the analytical result of Macek [10,11] (see also Federov and Jensen [9] and Efimov [1])

$$U_0(R)=\frac{15}{8\mu R^2}-\frac{4+t^2}{2\mu R^2}, \quad R\to\infty, \tag{4}$$

where $t=1.0062$. This result is independent of the details of the interparticle potential so long as it is short ranged with a zero energy bound state. A linear fit to our calculated three-body potential curve over the range 300 a.u.$<R<$700 a.u. gives $t=1.0042$ and is shown in the figure. If we additionally allow R^{-4} term, then a quadratic fit is necessary. Such a fit to our calculated curve over the range 100 a.u.$<R<$700 a.u. gives $t=1.0059$ and is shown in the figure. It is somewhat closer to the analytical result since it includes more points at smaller R which we can obtain with greater accuracy. The solutions to the hyperradial equation for this case will have energies which accumulate at $E=0$ as $E_v\approx E_0 e^{-\alpha v}$ where v is the vibrational quantum number and $\alpha=2\pi/t$. This follows solely from the fact that the potential is asymptotically R^{-2} [39–41].

For comparison, we have included in Fig. 9 the rescaled potential for $^4\mathrm{He}_3$. It is clear that the tail of this potential differs appreciably from the Efimov solution, Eq. (4). It follows that the Efimov character of the excited state of $^4\mathrm{He}_3$ cannot be explained in terms of the potential being locally R^{-2} as in Eq. (4). Presumably, though, as λ approaches $\lambda_{\mathrm{Efimov}}$ more and more closely, such a region would appear and grow. Finally, in Fig. 10 we show the channel functions for $\lambda=\lambda_{\mathrm{Efimov}}$. The probability density is spread throughout the (ϕ,θ) plane with some localization near the two-body potential wells as R increases. The essentially uniform distribution of probability — in contrast to the well localized probability for $^4\mathrm{He}_3$ (see Fig. 5) — persists for all R's and is a characteristic of Efimov states. In fact, it is precisely this behavior that leads to the long-range attraction peculiar to the Efimov effect.

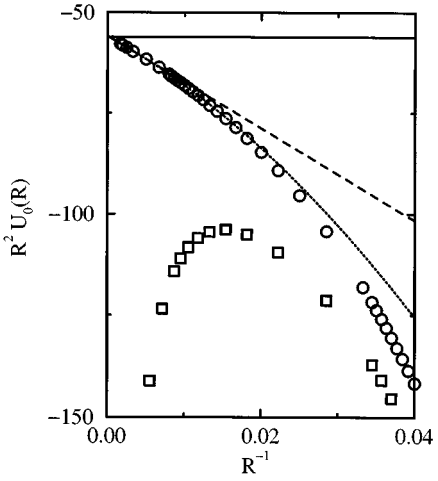

FIG. 9. A comparison of hyperspherical potential curves for $\lambda=\lambda_{\mathrm{Efimov}}$. Shown are the analytical result (solid line), the calculated points for the helium dimer interaction with $\lambda=\lambda_{\mathrm{Efimov}}$ (circles), the linear fit to the calculated points in the range 300 a.u. $<R<$700 a.u. (dashed line), and the quadratic fit to the calculated points in the range 100 a.u.$<R<$700 a.u. (dotted line). Also shown for reference is the $^4\mathrm{He}_3$ potential curve $\lambda=1$ (squares). The vertical axis is in a.u., the horizontal axis in a.u.^{2} K.

C. Halo states in the helium trimer

Recall that halo states of three particles occur for values of the interaction strength, λ, for which no two-body bound states exist. The upper limit on λ is clearly $\lambda_{\mathrm{Efimov}}$; the lower limit, λ_{halo}, must be determined by systematically reducing λ until no three-body bound state exists. For the helium trimer, we artificially reduce λ from $\lambda_{\mathrm{Efimov}}=0.9741$ to $\lambda_{\mathrm{halo}}=0.89$ [$\lambda_{\mathrm{halo}}=0.85$ neglecting $W_{00}(R)$]. Calculations [4,5] based upon some model short range two-body potentials have found an almost universal behavior for the ratio $\lambda_{\mathrm{halo}}/\lambda_{\mathrm{Efimov}}$. For example, $\lambda_{\mathrm{halo}}/\lambda_{\mathrm{Efimov}}=0.804$ for the Yukawa potential, $\lambda_{\mathrm{halo}}/\lambda_{\mathrm{Efimov}}=0.801$ for an exponential potential, and $\lambda_{\mathrm{halo}}/\lambda_{\mathrm{Efimov}}=0.794$ for a Gaussian potential. However, the ratio we find for the helium trimer, $\lambda_{\mathrm{halo}}/\lambda_{\mathrm{Efimov}}=0.91$, is significantly higher. This result is in agreement with the speculations of Goy *et al.* [5] concerning Morse interactions. They attribute the higher ratio to a large repulsive core in the two-body interaction which pushes the potential minimum to larger distances. The helium dimer potential (see Fig. 1) clearly shows such behavior with a minimum at about $r_{min}=5.6$ a.u. It is possible, though, that the difference might arise from the longer range r^{-6} behavior of the dimer potential rather than the exponentially decaying model potentials they had used. The channel functions for the halo states look very much like the $^3\mathrm{He}_3$ channel functions in Fig. 7 as the effective potentials show simi-

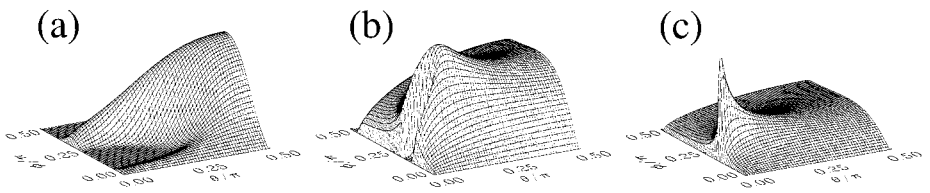

FIG. 10. The channel functions for $\lambda=\lambda_{\mathrm{Efimov}}$ plotted as $\sin\theta|\Phi_\nu(R;\phi,\theta)|^2$ for (a) $R=12$ a.u., (b) $R=50$ a.u., and (c) $R=500$ a.u. The vertical axis is a square-root scale.

lar features. Also, compared to Efimov states they do not have particularly large spatial extent.

IV. SUMMARY

We have applied the adiabatic hyperspherical method to the helium trimer and obtained results which are in excellent agreement with Fadeev approaches. Using one of the most accurate helium interaction potentials available, we find evidence for only one Efimov state in $^4He_3$. None of the isotopic combinations have Efimov states. In fact, only one, $^4He_2\,^3He$, has a bound state. Going beyond physical systems, we find that a reduction of the interaction strength to 97.4% of its physical value leads to an infinite number of Efimov states. In addition, the trimer has halo states for interaction strengths down to 89% of its physical value.

ACKNOWLEDGMENTS

This work was supported in part by the Department of Energy, Office of Basic Energy Sciences. C.D.L. was also partially supported by JILA and by the National Science Council of Taiwan.

[1] V. Efimov, Phys. Lett. **33B**, 563 (1970).
[2] V. Efimov, Nucl. Phys. **A210**, 157 (1973).
[3] V. Efimov, Comm. Nucl. Part. Phys. **19**, 271 (1990).
[4] J.M. Richard and S. Fleck, Phys. Rev. Lett. **73**, 1464 (1994).
[5] J. Goy, J.M. Richard, and S. Fleck, Phys. Rev. A **52**, 3511 (1995).
[6] M.V. Zhukov, B.V. Danilin, D.V. Federov, J.M. Bang, I.S. Thompson, and J.S. Vaagen, Phys. Rep. **231**, 151 (1993).
[7] D.V. Federov, A.S. Jensen, and K. Riisager, Phys. Rev. Lett. **73**, 2817 (1994).
[8] D.V. Federov, A.S. Jensen, and K. Riisager, Phys. Rev. C **49**, 201 (1994).
[9] D.V. Federov and A.S. Jensen, Phys. Rev. Lett. **71**, 4103 (1993).
[10] J. Macek, Z. Phys. D **3**, 31 (1986).
[11] Z. Zhen and J. Macek, Phys. Rev. A **38**, 1193 (1988).
[12] T. Cornelius and W. Glöckle, J. Chem. Phys. **85**, 3906 (1986).
[13] S. Huber, Phys. Rev. A **31**, 3981 (1985).
[14] T.K. Lim, S.K. Duffy, and W.K. Lambert, Phys. Rev. Lett. **38**, 341 (1977).
[15] H.S. Huber and T.K. Lim, J. Chem. Phys. **68**, 1006 (1978).
[16] S. Nakaichi-Maeda and T.K. Lim, Phys. Rev. A **28**, 692 (1983).
[17] T.K. Lim, Phys. Rev. A **34**, 4424 (1986).
[18] J.B. Anderson, C.A. Traynor, and B.M. Boghasian, J. Chem. Phys. **99**, 345 (1993).
[19] Y.H. Uang and W.C. Stwalley, J. Chem. Phys. **76**, 5069 (1982).
[20] B. Liu and A.D. McLean, J. Chem. Phys. **91**, 2348 (1989).
[21] F. Luo, G.C. McBane, G. Kim, C.F. Giese, and W.R. Gentry, J. Chem. Phys. **98**, 3564 (1993).
[22] F. Luo, C.F. Giese, and W.R. Gentry, J. Chem. Phys. **104**, 1151 (1996).
[23] W. Schöllkopf and J.P. Toennies, Science **266**, 1345 (1994).
[24] W. Schöllkopf and J.P. Toennies, J. Chem. Phys. **104**, 1155 (1996).
[25] R.A. Aziz, V.P.S. Nain, J.S. Carley, W.L. Taylor, and G.T. McConville, J. Chem. Phys. **70**, 4330 (1979).
[26] R.A. Aziz and M.J. Slaman, J. Chem. Phys. **94**, 8047 (1991).
[27] C.D. Lin, Phys. Rep. **257**, 1 (1995).
[28] Y. Zhou, C.D. Lin, and J. Shertzer, J. Phys. B **26**, 3937 (1993).
[29] U. Fano, Phys. Today **29**, 32 (1976).
[30] W.F. Ames, *Numerical Methods for Partial Differential Equations* (Academic Press, New York, 1992), p. 93.
[31] M.T. Jones and M.L. Patrick, NETLIB online documentation.
[32] J. Dongarra and E. Grosse, Commun. ACM **30**, 403 (1987). Available from NETLIB.
[33] M.T. Jones and M.L. Patrick, Appl. Numer. Math. **12**, 377 (1993).
[34] A. Starace and G.L. Webster, Phys. Rev. A **19** 1629 (1979).
[35] B.M. Axilrod and E. Teller, J. Chem. Phys. **11**, 299 (1943).
[36] C.A. Parish and C.E. Dykstra, J. Chem. Phys. **101**, 7618 (1994).
[37] I. Roeggen and J. Almlöf, J. Chem. Phys. **102**, 7095 (1995).
[38] F. Luo, G. Kim, C.F. Giese, and W.R. Gentry, J. Chem. Phys. **99**, 10084 (1993).
[39] M.J. Seaton, Proc. Phys. Soc. London **77**, 174 (1961).
[40] M. Gailitis and R. Damburg, Proc. Phys. Soc. London **82**, 192 (1963).
[41] C. H. Greene, Phys. Rev. A **20**, 656 (1979).
[42] B.D. Esry, Chris H. Greene, Y. Zhou, and C.D. Lin, J. Phys. B **29**, L51 (1996).